

Odyssey: An Automotive Lidar-Inertial Odometry Dataset for GNSS-denied situations

Journal Title
XX(X):1–9
©The Author(s) 2026
Reprints and permission:
sagepub.co.uk/journalsPermissions.nav
DOI: 10.1177/ToBeAssigned
www.sagepub.com/

SAGE

Aaron Kurda¹, Simon Steuernagel¹, Lukas Jung² and Marcus Baum¹

Abstract

The development and evaluation of Lidar-Inertial Odometry (LIO) and Simultaneous Localization and Mapping (SLAM) systems requires a precise ground truth. The Global Navigation Satellite System (GNSS) is often used as a foundation for this, but its signals can be unreliable in obstructed environments due to multi-path effects or loss-of-signal. While existing datasets compensate for the sporadic loss of GNSS signals by incorporating Inertial Measurement Unit (IMU) measurements, the commonly used Micro-Electro-Mechanical Systems (MEMS) or Fiber Optic Gyroscope (FOG)-based systems do not permit the prolonged study of GNSS-denied environments. To close this gap, we present *Odyssey*, a LIO dataset with a focus on GNSS-denied environments such as tunnels and parking garages as well as other underrepresented, yet ubiquitous situations such as stop-and-go-traffic, bumpy roads and wide open fields. Our ground truth is derived from a navigation-grade Inertial Navigation System (INS) equipped with a Ring Laser Gyroscope (RLG), offering exceptional bias stability characteristics compared to IMUs used in existing datasets and enabling the prolonged and accurate study of GNSS-denied environments. This makes *Odyssey* the first publicly available dataset featuring a RLG-based INS. Besides providing data for LIO, we also support other tasks, such as place recognition, through the threefold repetition of all trajectories as well as the integration of external mapping data by providing precise geodetic coordinates. All data, dataloader and other material is available online at <https://odyssey.uni-goettingen.de/>.

Keywords

Localization, Navigation, SLAM, Lidar-Odometry, Lidar-Inertial-Odometry, Intelligent Vehicles, Dataset

1 Introduction

Accurate and reliable localization is a key task for autonomous mobile systems. For outdoor applications such as autonomous driving, this is typically achieved via Global Navigation Satellite System (GNSS), which is based on relative position measurements to satellites. This, however, requires the robust reception of (weak) radio signals from suitable satellite constellations, which is not feasible in certain environments such as urban canyons or tunnels. The signals may even be actively disrupted by malicious actors. For these reasons, it is vital for autonomous vehicles to be able to continue accurate positioning in situations with (partial) GNSS loss.

A common approach in GNSS-denied situations is to solely rely on an Inertial Measurement Unit (IMU), which allows the calculation of the ego-pose (with respect to an initial pose) through the integration of linear acceleration and angular velocity measurements. This is known as strapdown inertial navigation (Budiyono 2012). Another common choice is to employ lidar data to estimate the ego motion of a mobile platform. This is called lidar odometry (Cadena et al. 2016; Lee et al. 2024). If the focus lies on constructing a (globally) accurate map of the surrounding, further methods for Simultaneous Localization and Mapping (SLAM) can be employed (Zhang et al. 2024). Assuming a (mostly) static environment, the transformation that aligns two consecutive point clouds with each other corresponds to the motion of the ego-vehicle. Similar to inertial navigation, these

motion increments can be integrated over time to result in the ego-pose with respect to a known origin. Recent works have explored the fusion of lidar odometry with inertial navigation, giving rise to the problem of Lidar-Inertial Odometry (LIO) (Shan et al. 2020; Malladi et al. 2025). While more robust, LIO methods suffer from the same problem as lidar odometry and inertial navigation: the accumulation of errors.

Two other directions that try to alleviate or entirely circumvent this problem have arisen in recent years. Map-assisted lidar odometry (Frosi et al. 2023; Kurda et al. 2025) tries to reduce the drift of lidar odometry through the integration of road networks or building outlines from third-party services such as OpenStreetMap. While certainly effective in suitable environments, once these methods diverge from their prior map, there are no mechanisms in place for them to recover. Place-recognition (Yin et al. 2025) on the other hand tries to circumvent this problem entirely. These methods aim to estimate the pose of the vehicle by comparing a single lidar scan against previously recorded scan or even a map of the region, allowing it to recognize

¹University of Göttingen, Göttingen, Germany

²iMAR Navigation, St. Ingbert, Germany

Corresponding author:

Aaron Kurda, Institute of Computer Science University of Göttingen, Göttingen, Germany

Email: aaron.kurda@cs.uni-goettingen.de

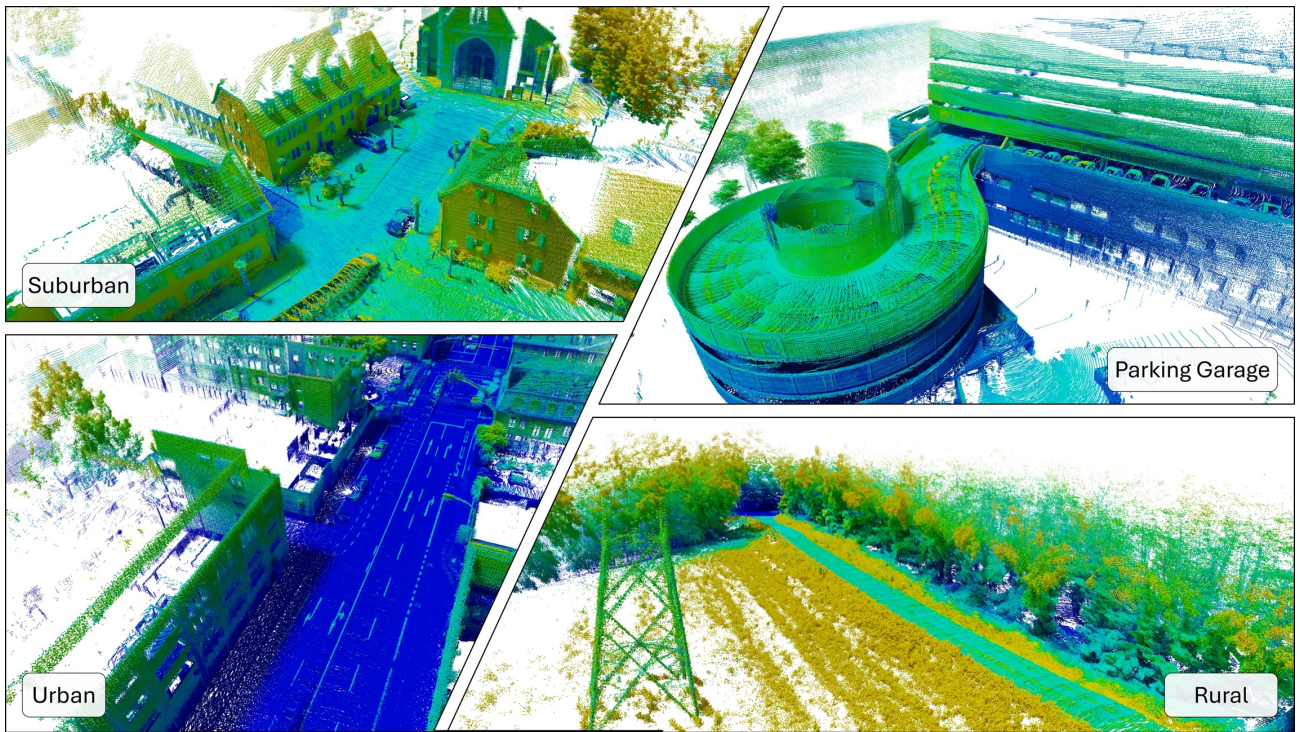


Figure 1. Example subset of the variety of environments included in the Odyssey dataset: Standard urban, suburban and rural environments as well as long-term GNSS-denied situation such as indoor parking garages and tunnels.

previously seen places (Yan et al. 2019; Cho et al. 2022). Compared to the map-assisted odometry methods, these approaches often require feature-rich, dense point cloud maps of the environment for a more robust and accurate localization (Dubé et al. 2020).

Regardless of the chosen localization approach, all methods rely on suitable data for their development and evaluation. Besides the lidar and inertial data for running a LIO algorithm, or the maps used by place-recognition methods, an accurate ground truth is required for assessing their performance. In many outdoor scenarios such ground truth can be obtained using a GNSS-augmentation system (Budiyono 2012) which, in combination with additional sensors such as IMUs, provide an accurate pose estimate independent of length and duration of the sequence. Receiving GNSS signals, however, ideally requires a clear, unobstructed view towards the sky and an absence of reflecting surfaces. This is not only a problem in tunnels or parking garages, but already (comparably) small buildings or short underpasses can cause a sporadic drop in accuracy. While alternative landmark-based localization system, such as roadside units, can be employed in smaller, controlled environments, equipping larger areas with such infrastructure quickly becomes infeasible. If no measurements to known landmarks can be received, the estimated position will slowly start to accumulate the IMUs measurement errors, resulting in a drifting trajectory (Budiyono 2012). While this drift can not be eliminated (without measurements to known landmarks), it can be reduced through the use of more accurate sensors.

The gyroscope is of special interest here, as its quality does not only influence the drifting behavior in GNSS-denied situations, but also the accuracy of the estimated orientation in general, even in situations with available GNSS-signals.

Due to the strong influence of the orientation on many of the commonly used error metrics such as the Relative Pose Error (RPE) and KITTI metric (Geiger et al. 2013), being able to more accurately estimate the orientation not only enables longer duration of GNSS-denied navigation, but also a more accurate evaluation overall.

1.1 Contribution

In this article, we present Odyssey, an automotive dataset tailored towards LIO. Odyssey is the first dataset which provides

- a highly accurate ground truth from a navigation-grade Ring Laser Gyroscope (RLG)-based Inertial Navigation System (INS),
- a large and diverse collection of environments with a special focus on prolonged GNSS-denied situations
- a separate IMU for a clean separation between ground truth and productive data for LIO, and
- support for map-assisted odometry and place recognition tasks.

Our ground truth is derived from a navigation-grade RLG-based INS that provides exceptional accuracy compared to the commonly used Micro-Electro-Mechanical Systems (MEMS) or Fiber Optic Gyroscope (FOG)-based systems, enabling us to provide very accurate ground truth orientation estimates for evaluation as well as data from prolonged GNSS-denied environments such as tunnels and parking garages. To the best of our knowledge, our dataset is the first dataset featuring such an RLG-based system. In total our dataset contains 12 trajectories, each repeated three times for a total of 36 sequences. The unique environments of the trajectories were chosen with the goal of providing a diverse and comprehensive sample of daily driving scenarios. They

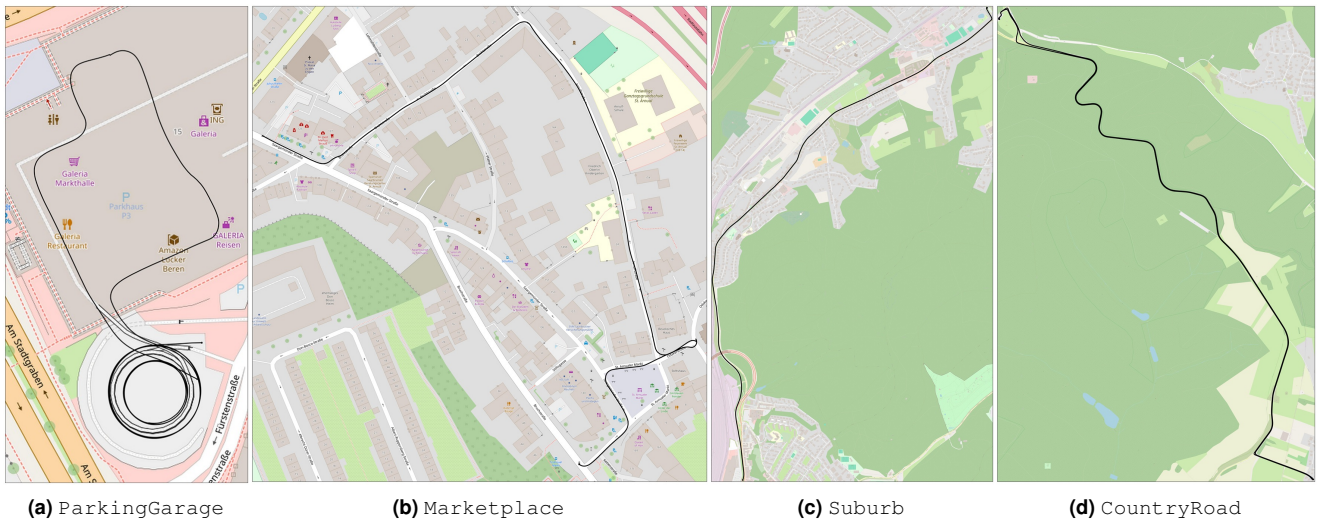


Figure 2. A subset of the trajectories overlaid with a rendering from OpenStreetMap, showing our dataset in urban, suburban and rural regions as well as in an indoor parking garage.

include parking garages, long tunnels, high-speed highways, urban and suburban environments, open fields and forest roads with thick vegetation and rough terrain. Odyssey also supports other localization tasks, such as map-assisted lidar odometry, by providing accurate geodetic coordinates for the integration of external mapping data, as well as place-recognition through the three-fold repetition for all our trajectories. To facilitate the development and evaluation of new methods, our website

<https://odyssey.uni-goettingen.de/>

provides a Python dataloader as well as other supplementary material. Furthermore, this article provides baseline results for some state-of-the-art lidar, lidar-inertial and map-assisted lidar odometry methods to validate our data and also provide baseline solutions for future works to compare against.

1.2 Structure

The remainder of this article is structured as follows: First, related work, including existing datasets for similar purposes, will be discussed in Section 2. Section 3 gives a detailed description of our dataset, including a short textual descriptions and summary statistics of the individual sequences (Section 3.1), a detailed description of our sensor suite used for data recording (Section 3.2) as well as a specification of the used data formats (Section 3.3). Lastly, in Section 4, we will provide baseline results for some publicly available lidar odometry, LIO as well as map-assisted lidar odometry methods.

2 RELATED WORK

One of the most established datasets is the KITTI Vision Benchmark Suite (Geiger et al. 2013), which also supports many other tasks such as visual odometry, optical flow or tracking tasks besides lidar odometry. Its lidar odometry (sub)-dataset comprises 22 sequences with a strong urban focus. However, due to the absence of a secondary IMU, this dataset is not suitable for LIO. ComplexUrban (Jeong

et al. 2019) and MulRan (Kim et al. 2020) are two more recent datasets. Opposed to KITTI, these include angular velocities and linear accelerations from a separate IMU. For ground truth generation, both datasets rely on a combination of Real-Time Kinematics GNSS (RTK GNSS), FOG and manual post-processing using loop closure detection of lidar scans. MulRan was originally designed for place-recognition and therefore features a threefold repetition of only four unique trajectories, resulting in 12 individual sequences. The main characteristic of the ComplexUrban dataset is its sensor arrangement, with four different rotating lidar sensors configured to maximum environmental coverage. A related dataset to ComplexUrban and MulRan is the Hong Kong UrbanNav (Hsu et al. 2023) dataset, which provides data of four different scenarios with a focus on urban-canyons. Similar to our dataset, it also features a long tunnel with few geometric features. It contains data from three spinning lidar scanners, a stereo camera and a secondary MEMS-based IMU. The ground truth is again derived from a fusion from RTK GNSS and FOG-based IMU measurements. ComplexUrban and UrbanNav provide simultaneous data from multiple lidar sensors that are arranged to deliver a comprehensive view of the surrounding environment. In contrast, the LIBRE dataset (Carballo et al. 2020) is designed to enable a systematic comparison between different lidar scanners. It uses a single mounting position, where the lidar sensor is exchanged between individual data acquisition runs. The dataset includes 10 distinct lidar scanners. Furthermore, IMU and GNSS measurements are available, although the dataset does not provide explicit ground-truth trajectories. HeLiPR (Jung et al. 2024) is a dataset tailored towards studying place recognition using different types of lidar scanners. Alongside its three original trajectories, it integrates seamlessly with MulRan by supplying new recordings of environments previously released as part of the MulRan dataset. Besides the data from four different spinning as well as solid-state lidars, the dataset contains a ground truth derived from a MEMS-based INS and additional inertial data. Similar to this, the EU long-term dataset (Yan et al. 2020) offer data from 11 different

Table 1. Summary statistics and short description for our 12 different trajectories. Length and Duration are averaged between individual repetitions and rounded while Total Sum corresponds to the sum of length and durations of the entire dataset.

Name	Length / m	Duration / s	Environment	Characteristics
Beltway	1751	221	urban	high speed, heavy traffic
CountryRoad	8764	700	rural	open field
ForestRoad	1636	346	rural	rough terrain, dense vegetation
Highway	12079	652	highway	high speed
HighwayTunnel	19465	900	highway	high speed, long tunnel
InnerCity	1251	369	urban	heavy traffic
Marketplace	868	221	sub-urban	rough terrain
ParkingGarage	607	254	sub-urban	indoor, spiral ramp
Suburb	4632	410	sub-urban	heavy traffic
Theatre	2549	351	urban	heavy traffic
Tunnel	470	305	urban	stop-and-go, tunnel
UndergroundCarPark	295	161	sub-urban	indoor
Total Sum	163099	14670		

lidar, radar and camera sensors with the goal of providing heterogeneous data for studying long-term autonomy for intelligent vehicles including adverse weather conditions among others. The ground truth is again derived from GNSS and IMU measurements. Adverse weather conditions have also been covered by the CADC (Pitropov et al. 2021) and the Boreas (Burnett et al. 2023) datasets. The CADC dataset contains 75 very short sequences of length between 50 to 100 lidar scans making it only partially usable for studying the drifting behavior of odometry methods. The Boreas dataset on the other hand contains 45 long trajectories of the same environment. While the evaluation of LIO methods is certainly possible, the single trajectory limits the needed diversity for a robust evaluation. While RLGs have been used to evaluate methods in past works (Georgy et al. 2012), there does currently no exist a publicly available dataset with ground truths derived from such a system.

In contrast to the car-mounted setup used for our dataset, a variety of datasets using other platforms such a mobile robots, handheld devices or backpacks-mounted system, have been proposed. The TIERS dataset (Qingqing et al. 2022) is recorded from a custom-built sensor platform that could be either mounted on a robot for motorized operation or manually pushed, depending on the environment. The platform carried 5 spinning and solid-state lidar scanners as well a lidar camera. No IMU or GNSS receivers were installed and the ground truth was instead obtained using Motion Capture (MOCAP) and SLAM systems. The dataset contains both outdoor and indoor scenarios, with the indoor scenarios limited to office areas and hallways. The Newer College (Ramezani et al. 2020) and, more recently, the Oxford Spires (Tao et al. 2025) datasets were captured using a handheld device. They cover indoor and outdoor environments in and around the Oxford campus, with ground truth generated by registering lidar scans against a prior map obtained from a static secondary lidar. A similar dataset was proposed in (Jin et al. 2025), containing lidar and inertial data collected using a custom backpack-mounted platform in both structured and unstructured environments. Unlike the Newer College and Oxford Spires datasets, its ground truth

is derived from a fusion of GNSS measurements and lidar-based mapping. Synthetic datasets generated using high-fidelity simulation, such as CarlaScenes (Kloukiniotis et al. 2022), have also been proposed. For the purposes of this work, however, we focus exclusively on real-world data and therefore do not discuss such datasets further.

3 THE ODYSSEY DATASET

The Odyssey dataset is divided into 12 trajectories, with each trajectory repeated three times, resulting in a total of 36 sequences. Rather than focusing on an individual environment as often done in modern datasets (Jeong et al. 2019; Kim et al. 2020), the deliberate decision was made to collect data from a diverse set of environments, as shown in Fig. 1 and Fig. 2. These range from urban canyons in densely inhabited cities, over suburbs with wide streets and detached houses, to rural regions with few to no artificial buildings. This diversity ensures our dataset captures the wide range of scenarios a vehicle may encounter in everyday traffic. In addition to such well-known scenarios, our dataset also contains rough, bumpy terrain and stop-and-go traffic for testing inertial odometry under sudden shocks and repeated acceleration and decelerations as well as challenging environments for lidar odometry systems, such as wide open fields, tight forest roads with thick vegetation, tunnels and parking garages with spiraling ramps. In total, our dataset comprises approximately 163 km of drive length and 4 h of drive duration.

3.1 TRAJECTORY DESCRIPTION

For easy identification, we use a similar nomenclature to the MulRan (Kim et al. 2020) and HeLiPR (Jung et al. 2024) datasets. For every distinct place/trajectory, we define a descriptive shorthand that reflects its content. An overview of all our trajectories including a short textual description as well as summary statistics can be found in the following enumeration as well as Table 1. For an even more detailed analysis, we additionally provide rendered videos of the lidar data for all sequences on our homepage.

Table 2. Overview of automotive datasets and their used gyroscopes. An \times denotes a missing secondary IMU

Dataset	1 st Gyro	1 st Gyro Bias Instability [°/h]	2 nd Gyro Bias Instability [°/h]	Data
KITTI (Geiger et al. 2013)	MEMS	2	\times	Urban
Complex Urban (Jeong et al. 2019)	FOG	0.05	10	Urban
MulRan (Kim et al. 2020)	FOG	0.05	10	Urban
UrbanNav (Hsu et al. 2023)	FOG	1	18	Urban
HeLIPR (Jung et al. 2024)	MEMS	0.45	10	Urban
EU Long Term (Yan et al. 2020)	MEMS	20	\times	Urban
Ours	RLG	0.001	0.8	Diverse



(a) Side View



(b) Trunk View

Figure 3. Vehicle and sensor setup used for recording the data, with the 360° lidar and estimate INS on top and the reference INS as well as the data collection system in the trunk. (Photos by iMAR Navigation GmbH)

- Beltway: A drive starting in the city and entering a beltway, featuring high speeds and a moderate amount of other traffic participants.
- CountryRoad: A drive that features a stretch of road through a forested region with a high embankment, followed by a wide open field with few trees and bushes.
- ForestRoad: A short round trip in and around a forest. It features thick vegetation, rough terrain and almost no artificial structures.
- Highway: A drive over a highway that starts in a suburban area. The drive features a moderate amount of traffic and some geometry deprived environments such as bridges.
- HighwayTunnel: A long drive over a highway. It contains a long circular tunnel that with no geometry for robust point cloud registration.
- InnerCity: An urban drive with many other traffic participants through the inner city of Saarbrücken.
- Marketplace: A suburban drive featuring a section of bumpy cobblestone road.
- ParkingGarage: An indoor parking garage with a spiraling entry.
- Suburb: A long trajectory that alternates between suburban and highway environments.
- Theater: An urban drive with comparably wide roads and a moderate amount of traffic.
- Tunnel: A short city tunnel without any geometry for longitudinal localization.
- UndergroundCarPark: A underground car park, similar to ParkingGarage.

3.2 SENSOR SUITE

The sensor suite for the Odyssey dataset contains

- an iPRENA-M-II (iMAR 2025), an RLG-based navigation-grade INS,
- an iNAT M300-TLE-LN1 (iMAR 2024), an automotive-grade MEMS-based INS,
- and an Ouster OS1 rev.7 (Ouster 2025), a 128-layer lidar.

Together, the iNAT M300-TLE-LN1 INS and Ouster OS1 form the productive subsystem that provides all data necessary for running LIO algorithms, i.e., lidar point clouds and IMU measurements. Data for evaluation, i.e., the ground truth, is provided by an entirely separate reference system, the iPRENA-M-II INS. A visualization of the vehicle used for data recording with the sensor setup is shown in Fig. 3 and a comparison between the gyroscopes used in our dataset and the gyroscopes used in other dataset is given in Table 2.

3.2.1 Lidar-Inertial Setup The lidar-inertial setup contains a 128-layer Ouster OS1 rev.7 (Ouster 2025) lidar and a iNAT M300-TLE-LN1 (iMAR 2024) INS. Both devices are mechanically fixed to each other and rigidly mounted on the roof of the vehicle (Fig. 3b). The lidar is operated at 10 Hz, yielding 128×2048 points per revolution. It is phase-synchronized to the Pulse Per Second (PPS)-signal of the iNAT M300-TLE-LN1 INS, which itself uses both GNSS signals as well as an internal oscillator for precise time keeping, even in GNSS-denied environments. The iNAT M300-TLE-LN1 is a MEMS-based INS that produces both pose and inertial estimates with a frequency of 300 Hz through the internal fusion of RTK GNSS signals and IMU measurements. However, since this dataset is tailored

towards LIO, we only the IMU data rather than the internally fused pose estimate of the INS.

3.2.2 Reference Setup The ground truth was recorded using an iPRENA-M-II (iMAR 2025), a navigation-grade INS system featuring a very precise RLG for orientation estimation. It produces pose and inertial estimates at a frequency of 250 Hz through internal fusion of RTK GNSS and IMU measurements. The main benefit of a RLG is its ability to accurately estimate its orientation over prolonged periods of time, which is one of the biggest sources of error in GNSS-denied environments. Here, both the bias instability as well as the sensor noise of our RLG as at least one order of magnitude lower compared to the best gyroscopes used in other datasets (Table 2). This increased accuracy enables us to provide more accurate pose estimates in GNSS-denied environments as well as more accurate orientational estimates in general.

Physically, the system is mounted in the trunk of the vehicle as shown in Fig. 3b, but the system's data output frame is already transformed to the lidar's origin to make the evaluation as comfortable as possible. For initial north-seeking, the system spent 20 minutes in a stationary alignment phase and for compensating initial sensor biases, the system was driven for a couple of kilometers before starting the recording. The linear acceleration and angular velocity measurements of both IMUs are recorded without any additional filtering. Only the in-house calibrated sensor errors are compensated to minimize potential adverse effects arising from filter cascading in real world LIO systems. All resulting quantities, i.e., orientations and position, however, are filtered to correct for the estimated sensor error during the recording process.

3.3 DATA FORMAT

The dataset is divided into 36 different sequences, labeled with a name corresponding to its trajectory, followed by a number indicating its repetition. The data of one sequence is sorted by sensor, as depicted in Fig. 4, with folder `refsy`s containing ground truth data from the reference system, `m300` containing IMU measurements from the productive system and `ouster` containing the point cloud from the lidar sensor. We additionally provide a folder `metadata` that contains useful data, statistics and visualizations for each sequence. The remainder of this section gives a detailed description of the data format necessary for reading the dataset. For convenience, we also provide a dataloader written in Python on our website.

3.3.1 IMU data format

All IMU data from one INS is saved as a single, both human and computer-readable Whitespace Separated Value (WSV) file. A single line corresponds to one IMU measurement, containing in order: the Unix timestamp t in nano-seconds since the 01.01.1970, the (filtered) orientation $[ori_x, ori_y, ori_z, ori_w]$ specified as a unit-quaternion with trailing scalar, the uncertainties in the orientation specified through the variances $[cov_{ori_00}, cov_{ori_11}, cov_{ori_22}]$, the angular velocities $[angvel_x, angvel_y, angvel_z]$ and the corresponding variances $[cov_{angvel_00}, cov_{angvel_11}, cov_{angvel_22}]$ and lastly the linear accelerations $[linacc_x, linacc_y, linacc_z]$ and the corresponding variances $[cov_{linacc_00}, cov_{linacc_11}, cov_{linacc_22}]$. Both the angular rates as well as the linear accelerations are provided raw, i.e., without any additional filtering. Only the in-factory calibrated sensor errors are compensated to minimize potential adverse effects arising from filter cascading in real-world LIO systems. The resulting quantities (orientations and positions), however, are filtered during the recording process to account for the estimated sensor errors.

3.3.2 NavSatFix data format All positional data from one INS is saved as a single, both human and computer-readable WSV file. A single line corresponds to one GNSS measurement, containing the 6 fields $[t, lat, lon, alt, cov_{00}, cov_{11}, cov_{22}]$ with t being the Unix time in nano-seconds, lat , lon and alt being the geodetic latitude and longitude in degrees, alt being the altitude above sea level in meters and $[cov_{00}, cov_{11}, cov_{22}]$ being the variances of lat , lon and alt respectively. The position $[lat, lon, alt]$ is an already filtered quantity from the fusion of the GNSS-signals and IMU measurements. The reference coordinate system for all geodetic coordinates is ETRS89/ETRF2024.

3.3.3 Lidar data format

Every full revolution of the lidar is saved as a binary file `ouster/<timestamp>.bin` with the filename indicating the Unix time in nano-seconds. Every lidar scan contains exactly 128×2048 lidar points sorted by laser (top to bottom) and time of acquisition. A single point is defined through a densely packed array of six 32-bit floating-point numbers $[x, y, z, t, reflectivity, near_ir]$ with x , y and z being the Euclidean coordinates in the front, left and up directions of the lidar itself, $t \in [0, 10000000]$ being the nano-seconds since the start of the revolution, $reflectivity \in [0, 255]$ being a measure of reflectivity of the surface that reflected the beam and $near_ir \in [0, 65535]$ being a measure of illumination.

The points of a lidar scan are ordered according to their beam of origin as well as their timestamp t within the scan. To fully preserve the structure of the scan, we included missing reflections through points containing all `nan` values.

3.3.4 Ground Truth data format

For the convenient evaluation of odometry algorithms, we additionally provide the ground truth poses synchronized with the acquisition times of the lidar point clouds as a WSV file `refsy/lidar_poses.txt`. The data format is identical to the KITTI data format, where every row contains the first three rows of a 4×4 homogenous transformation matrix specifying the orientation and translation of the vehicle w.r.t. the first pose, which is always set to the identity matrix. For time synchronization, we used the timestamps provided by the Ouster, and matched them to the closest ground truth pose timestamp. While the Ouster and our reference system do not output their measurements at exactly the same time, their clocks are synchronized through GNSS signals and internal oscillators, enabling the precise association between lidar scans and ground truth poses.

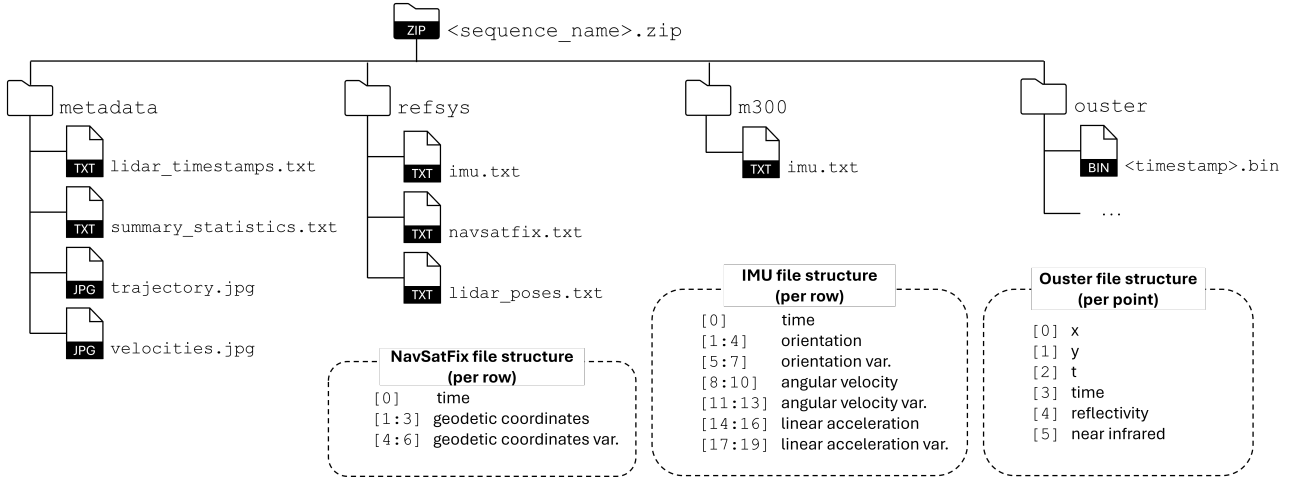


Figure 4. Folder and file structure of the Odyssey dataset. All data is divided by sensor. The folder `metadata` contains useful data and visualization of the sequence and the other folders contain the actual sensor data.

4 EVALUATION

For the validation of our data and for easy comparison for future works we provide the results of a multitude of publicly available localization methods on our data. These include the two lidar-only odometry methods KISS-ICP (Vizzo et al. 2023) and MAD-ICP (Ferrari et al. 2024), the LIO approach RKO-LIO (Malladi et al. 2025) as well as OSM-ICP (Kurda et al. 2025). For all methods we used the default parameters configuration as a baseline, modifying only the maximum and minimum ranges to 160 m and 3 m, respectively, and enabling scan deskew as a preprocessing step. All experiments were conducted on a laptop equipped with an Intel Core i7-1370P CPU and 32 GB of RAM. All data was stored on an external SSD. Under the chosen parameter settings, none of the methods reached real-time performance on our machine. Among them, KISS-ICP achieved the highest throughput of 9.58 FPS, followed by OSM-ICP and RKO-LIO with 7.70 and 7.46 FPS and lastly MAD-ICP with 5.79 FPS. We measured the accuracy for all methods using three different metrics: the RPE over sequences of the length of 100 m to evaluate the drifting behavior, the Absolute Pose Error (APE) for measuring the global consistency and lastly the frequently used KITTI metric (Geiger et al. 2013) that, similarly to the RPE, measures the drifting behavior of the system, but evaluates sequences of different lengths of up to 800 meters. For the calculation of the RPE and APE we used the `evo` Python package*, and for the calculation of the KITTI metric we used the official KITTI development kit†. Table 3 shows the results for all methods and all individual sequences.

The KITTI errors for all methods lie between 0.49 and 1.38 (excluding Tunnel and other outliers), placing their overall performance within a range comparable to results reported on other datasets. None of the approaches stand out as particularly problematic, yet their accuracy remains insufficient for applications demanding centimeter-level precision over long durations. The two GNSS-denied scenarios, `ParkingGarage` and `UndergroundCarPark`, do not exhibit any notable increase in difficulty; their error metrics remain well within the expected variance of the dataset. Overall none of the sequences stand out as particularly

problematic except Tunnel1. All methods report increased error values for both the KITTI and the RPE metric on this trajectory with the highest increase experienced on Tunnel1. A close inspection of the sequence reveals all methods to fail inside the tunnel while accelerating in stop-and-go traffic. A high amount of dynamic objects moving a coherent mass causes the methods wrongfully register them, instead of the (static) background. This problem is resolved for all methods once the tunnel is exited and the amount of static geometry increases. Even tunnels with little to no traffic can pose significant challenges with MAD-ICP additionally failing on Tunnel2 and KISS-ICP and OSM-ICP failing inside the tunnel on HighwayTunnel3. In Table 3, we marked all sequences/method combinations that exhibit this behavior in red.

5 CONCLUSION

In this work, we have presented a new dataset tailored towards lidar and lidar-inertial odometry. Its large scope covers a majority of standard driving situations from urban to rural situations. Through the use of a modern RLG-based INS we are additionally capable of providing data from genuine GNSS-denied environments including tunnels and, unprecedented, indoor parking garages. While the latter showed no notable increase in difficulty for lidar and lidar-inertial odometry methods, tunnels continue to pose substantial challenges. We provided multiple trajectories that caused state-of-the-art lidar and lidar-odometry methods to completely fail or at least suffer from decreased accuracy in these situations, revealing the necessity for the development of more robust approaches.

Acknowledgement

This work was funded by the German Federal Ministry for Economic Affairs and Climate Action (BMWK) within the research project “OKULAR” (Grant No. 19A22003C).

*<https://github.com/MichaelGrupp/evo>

†https://www.cvlibs.net/datasets/kitti/eval_odometry.php

Table 3. Results for a variety of different lidar, lidar-inertial and map assisted lidar odometry methods. We report the errors using the Absolute Pose Error (APE), the Relative Pose Error (RPE) over trajectory length of 100 m and the KITTI error metric. **Red** sequences indicate sequences with a significant deviation from the ground truth in individual situations, e.g., tunnels.

Sequence	KISS-ICP (Vizzo et al. 2023)			MAD-ICP (Ferrari et al. 2024)			RKO-LIO (Malladi et al. 2025)			OSM-ICP (Kurda et al. 2025)		
	APE	RPE	KITTI	APE	RPE	KITTI	APE	RPE	KITTI	APE	RPE	KITTI
Beltway1	10.93	1.15	1.06	11.89	1.18	1.09	11.59	1.20	1.05	8.27	0.83	0.69
Beltway2	10.13	1.13	1.06	11.23	1.16	1.01	7.03	1.19	1.01	8.48	0.79	0.67
Beltway3	12.40	1.16	1.15	11.52	1.21	1.13	6.96	1.21	1.08	8.50	0.83	0.71
CountryRoad1	112.23	1.13	1.23	45.86	1.21	1.04	91.50	1.20	1.03	68.42	0.76	0.73
CountryRoad2	133.70	1.13	1.31	56.48	1.23	1.09	110.52	1.21	1.06	79.45	0.78	0.78
CountryRoad3	140.49	1.14	1.32	51.04	1.23	1.05	109.25	1.21	1.06	81.10	0.77	0.80
ForestRoad1	9.15	0.77	1.24	6.07	0.85	0.77	8.29	0.77	0.88	6.32	0.62	0.84
ForestRoad2	8.80	0.77	1.32	4.37	0.80	0.72	5.36	0.76	0.92	5.97	0.59	0.86
ForestRoad3	10.09	0.85	1.38	5.32	0.93	0.83	12.08	0.85	1.01	6.42	0.70	0.93
Highway1	840.91	0.68	0.89	313.51	0.80	0.69	518.07	0.80	0.61	611.08	1.81	1.26
Highway2	827.63	0.74	0.90	342.46	0.82	0.71	487.28	0.84	0.63	433.68	0.61	0.49
Highway3	766.85	0.71	0.83	326.22	0.80	0.70	268.72	0.77	0.62	428.61	0.61	0.50
HighwayTunnel1	1415.01	0.64	1.08	666.94	0.76	0.69	656.40	0.76	0.75	601.90	0.63	0.58
HighwayTunnel2	1272.10	0.66	0.97	609.41	0.77	0.69	590.46	0.77	0.72	542.41	0.67	0.59
HighwayTunnel3	1455.85	8.60	4.02	700.29	0.77	0.69	700.68	0.77	0.77	799.03	5.36	2.93
InnerCity1	6.35	0.73	0.70	3.21	0.75	0.73	2.92	0.81	0.70	5.29	0.60	0.52
InnerCity2	3.21	0.93	0.72	2.96	0.93	0.77	62.56	1.01	0.82	2.77	0.74	0.52
InnerCity3	5.29	0.86	0.76	3.11	0.86	0.69	12.60	0.90	0.65	2.48	0.63	0.46
Marketplace1	2.81	0.94	1.04	2.51	0.97	1.06	16.09	1.22	1.25	2.17	0.62	0.65
Marketplace2	1.55	1.00	0.87	2.04	1.02	0.96	1.29	1.03	0.88	1.24	0.66	0.55
Marketplace3	1.95	1.17	1.01	1.89	1.19	1.06	1.59	1.20	1.00	1.29	0.74	0.62
ParkingGarage1	0.51	1.08	0.75	0.52	0.98	0.67	1.32	0.98	0.68	0.43	0.65	0.44
ParkingGarage2	0.55	1.15	0.80	0.46	0.93	0.65	0.52	0.98	0.68	0.44	0.66	0.45
ParkingGarage3	0.42	0.97	0.68	0.58	0.91	0.63	0.46	0.94	0.65	0.36	0.61	0.43
Suburb1	130.58	0.64	1.04	68.82	0.71	0.81	91.01	0.72	0.69	83.37	0.53	0.63
Suburb2	127.44	0.69	1.05	73.73	0.75	0.88	131.82	0.76	0.74	78.81	0.55	0.64
Suburb3	123.18	0.65	1.01	84.90	0.71	0.88	143.37	0.72	0.73	80.98	0.52	0.61
Theater1	24.13	0.91	0.87	20.40	0.93	0.81	60.88	0.95	0.74	16.55	0.67	0.56
Theater2	29.91	0.90	0.86	26.65	0.92	0.80	49.48	0.95	0.74	20.93	0.64	0.60
Theater3	22.68	0.93	0.88	18.81	0.94	0.85	18.31	1.00	0.76	17.34	0.68	0.60
Tunnel1	24.45	15.07	22.96	19.90	21.87	26.76	31.10	16.81	26.25	10.55	3.94	10.37
Tunnel2	5.15	2.45	3.13	16.66	6.72	7.92	2.16	1.36	0.95	1.03	0.96	0.73
Tunnel3	7.21	1.36	2.24	2.74	1.61	1.25	6.46	1.14	1.26	2.17	0.91	0.95
UndergroundCarPark1	0.48	0.94	0.81	0.54	0.87	0.70	0.88	0.90	0.79	0.43	0.62	0.57
UndergroundCarPark2	0.46	1.01	0.85	0.68	1.05	0.90	0.76	1.00	0.85	0.37	0.66	0.57
UndergroundCarPark3	0.41	0.94	0.79	0.67	0.97	0.82	0.77	0.93	0.78	0.35	0.63	0.55

References

Budiyono A (2012) Principles of GNSS, inertial, and multi-sensor integrated navigation systems. *Industrial Robot: An International Journal* 39(3).

Burnett K, Yoon DJ, Wu Y, Li AZ, Zhang H, Lu S, Qian J, Tseng WK, Lambert A, Leung KY, Schoellig AP and Barfoot TD (2023) Boreas: A multi-season autonomous driving dataset. *The International Journal of Robotics Research* 42(1-2): 33–42.

Cadena C, Carlone L, Carrillo H, Latif Y, Scaramuzza D, Neira J, Reid I and Leonard JJ (2016) Past, present, and future of simultaneous localization and mapping: Toward the robust-perception age. *IEEE Transactions on Robotics* 32(6): 1309–1332.

Carballo A, Lambert J, Monrroy A, Wong D, Narksri P, Kitsukawa Y, Takeuchi E, Kato S and Takeda K (2020) LIBRE: The multiple 3D lidar dataset. In: *2020 IEEE Intelligent Vehicles symposium (IV)*. IEEE, pp. 1094–1101.

Cho Y, Kim G, Lee Sm and Ryu JH (2022) OpenStreetMap-based lidar global localization in urban environment without a prior lidar map. *IEEE Robotics and Automation Letters* 7: 1–1. DOI: 10.1109/LRA.2022.3152476.

Dubé R, Cramariuc A, Dugas D, Sommer H, Dymczyk M, Nieto J, Siegwart R and Cadena C (2020) SegMap: Segment-based mapping and localization using data-driven descriptors. *The International Journal of Robotics Research* 39(2-3): 339–355.

Ferrari S, Di Giammarino L, Brizi L and Grisetti G (2024) MAD-ICP: It is all about matching data-robust and informed lidar odometry. *IEEE Robotics and Automation Letters* DOI:10.1109/LRA.2024.3456509.

Frosi M, Gobbi V and Matteucci M (2023) OSM-SLAM: Aiding SLAM with OpenStreetMaps priors. *Frontiers in Robotics and AI* 10. DOI:10.3389/frobt.2023.1064934.

Geiger A, Lenz P, Stiller C and Urtasun R (2013) Vision meets robotics: The KITTI dataset. *The International Journal of Robotics Research* 32(11): 1231–1237.

Georgy J, Noureldin A and Goodall C (2012) Vehicle navigator using a mixture particle filter for inertial sensors/odometer/map data/gps integration. *IEEE Transactions on Consumer Electronics* 58(2): 544–552. DOI:10.1109/TCE.2012.6227459.

Hsu LT, Huang F, Ng HF, Zhang G, Zhong Y, Bai X and Wen W (2023) Hong kong UrbanNav: An open-source multisensory dataset for benchmarking urban navigation algorithms. *NAVIGATION: Journal of the Institute of Navigation* 70(4).

iMAR (2024) *iNAT-M300/TLE-LN1*. iMAR Navigation and Control. URL https://www.imar-navigation.de/de/component/zoo/?task=callelement&format=raw&item_id=1291&element=064031b9-6fdb-40ba-a750-74bf928e03ec&method=download. Rev. 1.19.

iMAR (2025) *iPRENA-II /-IIIA/ -III /-IV*. iMAR Navigation and Control. URL https://www.imar-navigation.de/en/component/zoo/?task=callelement&format=raw&item_id=906&element=064031b9-6fdb-40ba-a750-74bf928e03ec&method=download. Rev. 2.07.

Jeong J, Cho Y, Shin YS, Roh H and Kim A (2019) Complex urban dataset with multi-level sensors from highly diverse urban environments. *The International Journal of Robotics Research* 38(6): 642–657.

Jin X, Bu N, Wang S, Ge J, Xiao J and Matteucci M (2025) Large-scale lidar-inertial dataset for degradation-robust high-precision mapping. URL <https://arxiv.org/abs/2507.20516>.

Jung M, Yang W, Lee D, Gil H, Kim G and Kim A (2024) HeLiPR: Heterogeneous lidar dataset for inter-lidar place recognition under spatiotemporal variations. *The International Journal of Robotics Research* 43(12): 1867–1883.

Kim G, Park YS, Cho Y, Jeong J and Kim A (2020) MuIRan: Multimodal range dataset for urban place recognition. In: *2020 IEEE International Conference on Robotics and Automation (ICRA)*. IEEE, pp. 6246–6253.

Kloukiniotis A, Papandreou A, Anagnostopoulos C, Lalos A, Kapsalas P, Nguyen DV and Moustakas K (2022) CarlaScenes: A synthetic dataset for odometry in autonomous driving. In: *Proceedings of the IEEE/CVF Conference on Computer Vision and Pattern Recognition (CVPR) Workshops*. pp. 4520–4528.

Kurda A, Steuernagel S, Jung L and Baum M (2025) Reducing drift of lidar odometry by incorporating OpenStreetMap building data. In: *2025 European Conference on Mobile Robots (ECMR)*. Padua, Italy: IEEE.

Lee D, Jung M, Yang W and Kim A (2024) Lidar odometry survey: Recent advancements and remaining challenges. *Intelligent Service Robotics* 17(2): 95–118.

Malladi MVR, Guadagnino T, Lobefaro L and Stachniss C (2025) A robust approach for lidar-inertial odometry without sensor-specific modeling. URL <https://arxiv.org/abs/2509.06593>.

Ouster (2025) *OS1 Mid-Range High-Resolution Imaging Lidar*. Ouster. URL <https://data.ouster.io/downloads/datasheets/datasheet-rev7-v3p1-os1.pdf>. Rev. 02/2025.

Pitropov M, Garcia DE, Rebello J, Smart M, Wang C, Czarnecki K and Waslander S (2021) Canadian adverse driving conditions dataset. *The International Journal of Robotics Research* 40(4–5): 681–690.

Qingqing L, Xianjia Y, Queraltá JP and Westerlund T (2022) Multi-modal lidar dataset for benchmarking general-purpose localization and mapping algorithms. In: *2022 IEEE/RSJ International Conference on Intelligent Robots and Systems (IROS)*. IEEE, pp. 3837–3844.

Ramezani M, Wang Y, Camurri M, Wisth D, Mattamala M and Fallon M (2020) The newer college dataset: Handheld lidar, inertial and vision with ground truth. In: *2020 IEEE/RSJ International Conference on Intelligent Robots and Systems (IROS)*. IEEE, pp. 4353–4360.

Shan T, Englot B, Meyers D, Wang W, Ratti C and Daniela R (2020) LIO-SAM: Tightly-coupled lidar inertial odometry via smoothing and mapping. In: *IEEE/RSJ International Conference on Intelligent Robots and Systems (IROS)*. IEEE, pp. 5135–5142.

Tao Y, Muñoz-Bañón MÁ, Zhang L, Wang J, Fu LFT and Fallon M (2025) The Oxford spires dataset: Benchmarking large-scale lidar-visual localisation, reconstruction and radiance field methods. *International Journal of Robotics Research*.

Vizzo I, Guadagnino T, Mersch B, Wiesmann L, Behley J and Stachniss C (2023) KISS-ICP: In defense of point-to-point ICP - simple, accurate, and robust registration if done the right way. *IEEE Robotics and Automation Letters* 8(2): 1029–1036.

Yan F, Vysotska O and Stachniss C (2019) Global localization on OpenStreetMap using 4-bit semantic descriptors. In: *2019 European Conference on Mobile Robots (ECMR)*. pp. 1–7. DOI:10.1109/ECMR.2019.8870918.

Yan Z, Sun L, Krajník T and Ruicheck Y (2020) EU long-term dataset with multiple sensors for autonomous driving. In: *2020 IEEE/RSJ International Conference on Intelligent Robots and Systems (IROS)*. IEEE, pp. 10697–10704.

Yin P, Jiao J, Zhao S, Xu L, Huang G, Choset H, Scherer S and Han J (2025) General place recognition survey: Toward real-world autonomy. *IEEE Transactions on Robotics* 41: 3019–3038. DOI:10.1109/TRO.2025.3550771.

Zhang Y, Shi P and Li J (2024) 3d lidar slam: A survey. *The Photogrammetric Record* 39(186): 457–517.